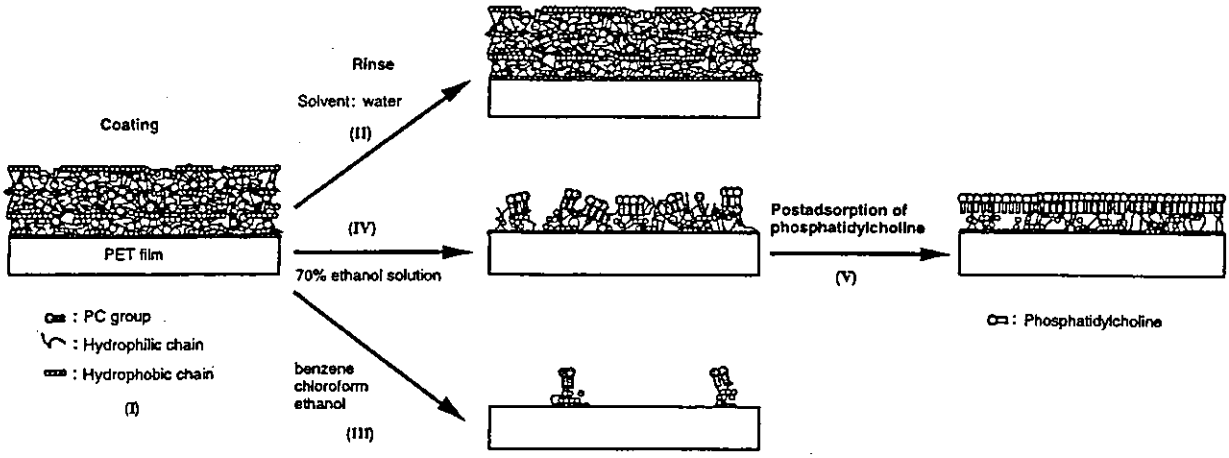

Fig. 8. Schematic of configurations of phosphorylcholine-bearing co-oligomer coatings. (I) Cast from solution and air-dried. Relatively thick, disorganized multilayers where the outer surface is enriched with hydrophobic block oligoST. (II) Washing with water causes neither desorption of excess oligomers nor rearrangement of layers. (III) Washing with hydrophobic and polar solvents removes almost completely the adsorbed multilayers, leaving a very small fraction of oligomers on the surface. (IV) Washing with 70% ethanolic solution considerably removes excess oligomers from the surface, leaving a monolayered oligomer on the surface, in which hydrophobic oligoST anchors on the surface, and PC groups, assembled by hydrophobic association of alkane groups, are exposed to the water/substrate interface. (V) Upon addition of a small amount of phospholipid, followed by washing with 70% ethanolic solution, co-organized layers closely packed with PC groups at the outermost surface layer are formed.

due to adsorption of phosphatidylcholine to the PC-assembled surface (V).

3.4. Surface plasmon resonance analysis for protein adsorption

Protein adsorption characteristics on the co-oligomer (5)-coated surface, that was prepared by coating with aqueous solution and subsequent rinsing with 70% ethanolic solution, were determined using IgG as a model protein under flow conditions, and compared with those on two different SAM surfaces that were prepared by the self-assembly of corresponding alkanethiol with the OH- or CH_3-group at the head of the molecules, according to the method previously reported. XPS analysis showed that the surface was covered by respective alkanethiolates, which was reported [12] in our previous paper [12]. Fig. 9 shows the SPR profiles that describe time-dependent changes of resonance angle shift, which is related to the quantity of protein adsorbed on the co-oligomer-coated surface (a), OH-SAM surface (b), and the CH_3-SAM surface (c). The initial adsorption rate on the CH_3-SAM surface was the highest, followed by those on the OH-SAM surface and the co-oligomer (5)-coated surface. However, a slightly reduced IgG adsorption rate was noted for the co-oligomer (5)-coated surface at around 4 h flow as compared with those on the other two SAM surfaces.

3.5. Cell adhesion

ECs were seeded and cultured on co-oligomer (5)-coated substrates (gold-plated glass) for up to 24 h.

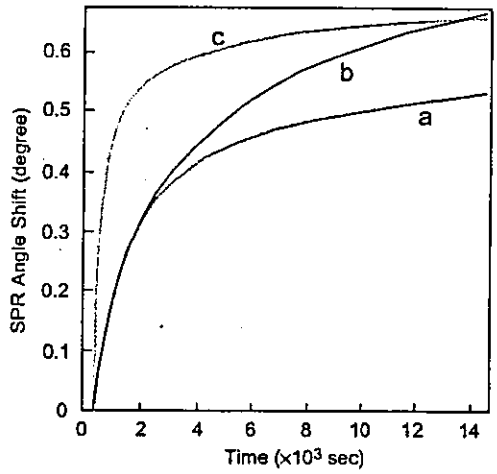

Fig. 9. Shift of resonance angles in SPR spectroscopy upon IgG adsorption for three self-assembled surfaces on gold substrates: (a) co-oligomer (5)-coated surface, (b) OH-SAM surface, and (c) CH_3-SAM surface. Measurement conditions: up to 4 h, 0.1 mg/ml IgG buffer solution, and a flow rate of 100 μl/ml.

Fig. 10 shows time-dependent changes in number of the adhered cells on substrates that were pre-coated with co-oligomer (5) and subsequently rinsed with 70% ethanolic solution or chloroform. The degree of adhesion was found to decrease as follows: commercial tissue culture dish > non-coated gold substrate > chloroform-rinsing coated gold substrate ≫ 70% ethanol solution-rinsing coated gold substrate. In order to determine how EC adhesion is suppressed in serum-containing medium, the substrates were pretreated with the mixed buffered

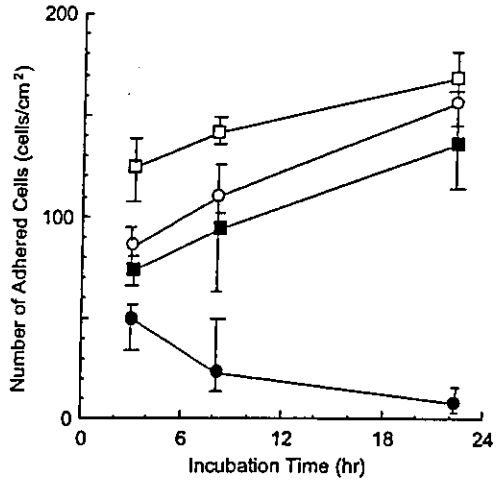

Fig. 10. EC adhesion on various surfaces: tissue culture dish (□), non-coated gold surface (○), PC-bearing oligoDMAAm–oligoST (5)-coated surface after washing with chloroform (■), and 70% ethanolic is solution (●) ($n = 3$).

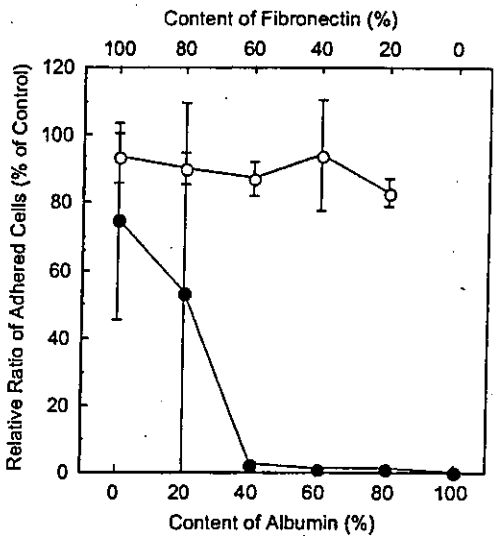

Fig. 11. Pre-adsorbed fibronectin-dependent EC adhesion on PC-oligoDMAAm–oligoST (5)-coated surface pretreated with 10 μg/ml of mixed protein solution containing fibronectin and albumin, in comparison with that on tissue culture dishes: tissue culture dish (○), and PC-oligoDMAAm–oligoST (5)-coated surface (●).

solution of fibronectin (FN, a potent cell-adhesive protein) and albumin (Alb, non-cell-adhesive protein) at various mixing ratios, and ECs were cultured for 3 h. Fig. 11 shows the relationship between number of adhered cells and FN fraction in the mixed solution. The increase in the ratio of Alb to FN drastically reduced cell adhesion on the co-oligomer-coated substrate. When the Alb fraction in the solution exceeded 60%, no adhesion was observed, whereas there was little difference in cell adhesion on commercial tissue culture dishes coated with the mixed protein solutions with different mixing ratios.

4. Discussion

The concept of surface biocompatibility among various biomimetic approaches has evolved from the study of cell membranes. The systematic research conducted by Chapman et al. suggested that among phospholipids with various ionic head groups, the PC head group is only one responsible for blood compatibility. This is based on the fact that phospholipids with an electrically neutral PC head group (phosphatidylcholine and sphingomyelin) are predominant in the outer half of the bilayer of cell membranes, while negatively charged phosphatidylserine is almost exclusively found in the inner half of the bilayer. Since densely distributed PC polar head groups exist in the outer lipid surface of red blood cells which are only one cell type of non-adhesivity toward substrates among blood cells, it has been hypothesized that the existence of PC head groups on substrates may provide high non-cell adhesivity. The PC head groups are very polar but electrically neutral under physiological conditions, due to zwitterions that can bind a large amount of water. Macroudas hypothesized almost three decades ago that low adhesiveness of phospholipid substrate is due to increased entropy of adsorbed water and hence decreased entropic driving force for polymer to displace water from a fluid interface [13]. A molecular dynamics study concluded that the first layer of water molecules at the interface with PC head group is highly polarized and that there are heavy, non-random associations of water molecules with the head groups [14,15,22]. This very strong hydration effect was experimentally evidenced by neutron reflection study that revealed that outermost layer of PC-bearing vinyl polymer was mixed with approximately 85% water [16].

PC groups have a strong tendency to form a closely packed monolayer as a result of electrostatic interaction between adjacent PC groups. A simple geometric argument indicates that an almost parallel orientation of PC polar head groups that form a six-membered inner salt as a result of electrostatic attraction between adjacent PC polar head groups brings oppositely charged groups close to each other, resulting in almost complete neutralization. The arrayed PC polar head groups must have formed a very strong hydration shell around the packed head groups, which may create a steric barrier prohibiting protein adsorption [23]. Thus, the closely packed PC head groups surface is thought to be very highly swollen, highly hydrophilic and strongly hydrated [16,22]. Therefore, if a spatial density of the PC polar head groups is increased and supramolecular assembly forming a closely packed configuration is

realized on a surface, such a surface may lead to minimal or reduced biological reactivity unless an entropy effect arising from either dehydration of the surface or protein molecules or change in the formation of protein molecules during adsorption has not considerably contributed to the full energy change.

Extensive molecular designs of PC-bearing polymer surface or PC self-assembled layer include polymerized phospholipids [11,17], copolymers having PC groups in their side chains (for example, copolymer of 2-acryloxyethyl phosphorylcholine with (meth)acrylates with hydrophobic side chains), and thiol- or disulfide-bearing PCs [18]. The former (co)polymers were cast on various substrates, whereas the latter thiol- or disulfide-bearing PCs formed an SAM on gold via chemisorption. In terms of the surface density of the PC polar head groups, the surface density of the former (co)polymers was much lower than that of the latter. However, very hydrophilic PC head groups exist at the interface between water and the coated polymer. In addition, a hypothesis was formulated that phospholipids present in blood are adsorbed on the PC-bearing surface to form self-assembled PC-rich surfaces, which results in a markedly reduced protein adsorption [7,8]. The other interesting molecular design of PC-bearing lipid with a hydrophilic polymer spacer was prepared by in situ photoiniferter polymerization initiated from lipid assembly coupled to PC-bearing iniferter [12].

Our design approach is to prepare oligomer-based PC-bearing surfactants in which a PC polar head group with a long alkylene chain, $(CH_2)_{11}$, is installed in one end of a molecule. Hydrophobic intermolecular association of alkylene chains may drive the self-assembly of PC polar head groups. OligoST was used as a hydrophobic anchoring segment on substrates in water. In order to avoid the hydrophobic interaction of the alkylene chain with the anchoring oligoST segment (if this happens, a disorganized layer may be formed), a water-soluble segment composed of oligoDMAAm was inserted between the oligoST segment and the PC head group. This molecular architecture was realized by "quasi-living" photopolymerization using the unique photochemical reactivity of dithiocarbamate as evidenced by the controlled molecular architecture of block copolymers [9,19,20]. Since the PC head group was incorporated to the photoiniferter molecule, a PC head group exists at the starting end of the oligomer or the co-oligomer. As shown in Fig. 3, the chain lengths of the oligomers were easily controlled by adjusting the photoirradiation time at fixed concentrations. Similarly, Kitano et al. [21] prepared PC-bearing polymers with long hydrocarbon tails via the iniferter technique to form liposomes.

The co-oligomer, after being cast on the substrate and subsequent rinsing with water, may form a multilayer on the surface due to the inter- and intramolecular hydrophobic interactions of oligoST blocks by themselves (Fig. 5), which was deduced from the unexpectedly high advancing contact of angle 92° and the relatively low receding angle of 28° (Table 2). After washing with benzene, chloroform and ethanol, most of the adsorbed multilayered co-oligomers appeared to be washed off, thus leaving a very small amount of adsorbed molecules. However, rinsing with 70% ethanolic solution considerably lowered both advancing and receding angles (73° and 14°, respectively), concomitantly minimizing the hysteresis of contact angles. This suggests that by such a rinsing, a monolayered configuration of co-oligomer is formed on the substrate, where oligoST is anchored on the substrate and the PC head group preferentially ends up on the outermost layer. It is speculated that intermolecularly associated alkylene chains form a supramolecular assembly. Furthermore, immersion into dipalmitoryl phosphatidylcholine-containing aqueous solution also gave low contact angles, suggesting that the phospholipid appears to be inserted in the hydrophobic palisade of monolayered PC-bearing co-oligomers, resulting in the formation of a co-organized PC-bearing layer. On the other hand, rinsing with more hydrophobic solvents such as chloroform, ethanol and benzene resulted in an almost complete desorption of PC-bearing co-oligomers from the substrates. Although it is not sure how long such a co-oligomer adsorbed on the surface remains in blood under the working conditions of an implanted device, it is expected that the short-term use of an extracorporeal circulatory device, in which a blood-contacting surface is properly coated, may guarantee a highly antithrombogenic potential.

It is of paramount interest to know whether PC head groups exert the non-adsorptive, minimally adsorptive or reduced adsorptive characteristic of protein, irrespective of cell-adhesive proteins, such as fibronectin (FN) or vitronectin (VN), or non-cell-adhesive proteins, such as albumin (Alb), and whether the PC head groups has a non-adsorptive characteristic particularly specific to cell-adhesive proteins. Literature indicates that there are confronting experimental results on protein adsorption. Some studies have evidenced that PC head groups-bearing surfaces reduced protein adsorption, regardless of type of proteins. Ellipsometric measurements have shown that the amount of protein PC-bearing surfaces is lower than that of non-treated surfaces [16].

On the other hand, for the chemisorbed phospholipid monolayer on gold, quantitative measurements employing radiolabeled FN showed that FN adsorbed well on PC-chemisorbed gold surfaces in a manner similar to that on non-treated gold surfaces. Moreover, substantial cell adhesion was observed for FN- and VN-coated surfaces [18], whereas cell adhesion on albumin-treated surfaces was minimal.

The present preliminary experiments on cell adhesion assay and protein adsorption characteristics using SPR measurements showed that competitive adsorption in a mixed solution of Alb and FN is favored for the preferential adsorption of Alb, which was deduced from the cell adhesion assay (Fig. 8), whereas, in in situ real-time measurements using SPR, IgG adsorption was only slightly reduced as compared with those on hydrophobic (methyl group-packed) and hydrophilic (hydroxyl-group-packed) surfaces (Fig. 6). These results may imply that the PC head group-assembled surface adsorbs preferentially non-adhesive proteins in serum-containing medium. Regardless of the non-specific, reduced protein-adsorptive characteristic or the specific non-adsorptive characteristic for cell-adhesive proteins, a markedly reduced adhesion of various types of cells including platelets [8], neutrophils [8] and ECs (present study) was observed on PC-bearing surfaces in serum-containing medium or blood. Future study should be directed at elucidating the mechanism involved in the repelling action for protein adsorption on PC-bearing self-assembled surfaces.

Acknowledgements

This study was financially supported by the Promotion of Fundamental Studies of Health Science of the Organization for Pharmaceutical Safety and Research (OPSR) under grant no. 97-15, and in part by a Grant-in-Aid for Scientific Research (A2-12358017, B2-12470277) from Ministry of Education, Culture, Sports, Science, and Technology of Japan.

References

[1] Hayward JA, Chapman D. Biomembrane surfaces as models for polymer design: the potential for haemocompatibility. Biomaterials 1984;5:135–42.
[2] Durrani AA, Hayward JA, Chapman D. Biomembrane as models for polymer surfaces. II. The syntheses of reactive species for covalent coupling of phosphorylcholine to polymer surfaces. Biomaterials 1986;7:121–5.
[3] Hayward JA, Durrani AA, Shelton J, Lee DC, Chapman D. Biomembranes as models for polymer surfaces. III. Characterization of a phosphorylcholine surface covalently bound to glass. Biomaterials 1986;7:126–31.
[4] Hayward JA, Durrani AA, Lu Y, Clayton CR, Chapman D. Biomembranes as models for polymer surfaces IV ESCA analysis of a phosphorylcholine surface covalently bound to hydroxylated substrates. Biomaterials 1986;7:252–8.
[5] Kadoma Y, Nakabayashi N, Masuhara E, Yamauchi J. Synthesis and hemolysis test of the polymer containing phosphorylcholine groups. Kobunshi Ronbunshu 1978;35:423–7.
[6] Kojima M, Ishihara K, Watanabe A, Nakabayashi N. Interaction between phospholipids and biocompatible polymers containing phosphorylcholine moiety. Biomaterials 1991;12:121–4.
[7] Ishihara K, Ziats NP, Tierney BP, Nakabayashi N, Anderson JM. Protein adsorption from human plasma is reduced on phospholipid polymer. J Biomed Mater Res 1991;25:1397–407.
[8] Iwasaki Y, Kurita K, Ishihara K, Nakabayashi N. Effect of reduced protein adsorption on platelet adhesion at the phospholipid polymer surface. J Biomater Sci Polym Edn 1996;8:151–63.
[9] Otsu T, Yoshida M. Role of initiator-transfer agent-terminator (iniferter) in radical polymerizations: polymer design by organic disulfides as iniferters. Makromol Chim: Rapid Commun 1982;3:127–32.
[10] Durrani AA, Chapman D. Modification of polymer surfaces for biomedical applications. In: Polymers surfaces and interfaces. New York: Wiley; 1987 [Chapter 10].
[11] Ruiz L, Hilborn JG, Leonard D, Mathieu HJ. Synthesis, structure and surface dynamics of phosphorylcholine functional biomimicking polymers. Biomaterials 1998;19:987–98.
[12] Niwa M, Data M, Higashi N. In situ photopolymerization of methacrylic acid at a self-assembled xanthate monolayer surface on gold. Formation of poly(methacrylic acid) brushes and their interaction with cytochrom c. Macromolecules 1996;26:3681–5.
[13] Maroudas NG. On the low adhesiveness of fluid phospholipid substrata. J Theor Biol 1979;79:101–16.
[14] Malmsten M. Ellipsometry studies of protein adsorption at lipid surfaces. J Colloid Interface Sci 1994;168:247–54.
[15] Malmsten M. Protein adsorption at phospholipid surfaces. J Colloid Interface Sci 1995;172:106–15.
[16] Murphy EF, Lu JR, Brewer J, Russell J, Penfold J. The reduced adsorption of proteins at the phosphorylcholine incorporated polymer–water interface. Langmuir 1999;15:1313–22.
[17] Marra KG, Winger TM, Hanson SR, Chaikof EL. Cytomimetic biomaterials. 1. In-situ polymerization of phospholipids on an alkylated surface. Macromolecules 1997;30:6483–8.
[18] Coyle LC, Danilov YN, Juliano RL, Regen SL. Chemisorbed phospholipid monolayers on gold: well-defined and stable phospholipid surfaces for cell adhesion studies. Chem Mater 1989;1:606–11.
[19] Nakayama Y, Miyamura Y, Hirano Y, Goto K, Matsuda T. Preparation of poly(ethylene glycol)–polystyrene block copolymers using photochemistry of dithiocarbamate as a reduced cell adhesive coatings. Biomaterials 1999;20:963–70.
[20] Nakayama Y, Matsuda T. Surface macromolecular microarchitecture design: biocompatible surfaces via photo-graft-copolymerization using *N,N*-dithiocarbamate. Langmuir 1999;15:5560–6.
[21] Kitano H, Chibashi M, Nakamata S, Ide M. Block telomer-carrying amphiphiles prepared with a phospholipid iniferter. Langmuir 1999;15:2709–13.
[22] Sheng Q, Schulten k, Pidgeon C. Molecular dynamics simulation of immobilized artificial membranes. J Phys Chem 1995;99: 11018–27.
[23] Zhang SF, Rolfe P, Wright G, Lian W, Milling AJ, Tanaka S, Ishihara K. Physical and biological properties of compound membranes incorporating a copolymer with a phosphorylcholine head group. Biomaterials 1998;19:691.

Novel Visible-Light-Induced Photocurable Tissue Adhesive Composed of Multiply Styrene-Derivatized Gelatin and Poly(ethylene glycol) Diacrylate

Cailong Li,[1,2] Toshinobu Sajiki,[1] Yasuhide Nakayama,[3] Masashi Fukui,[2] Takehisa Matsuda[1]

[1] Department of Biomedical Engineering, Graduate School of Medicine, Kyushu University, 3-1-1 Maidashi, Higashiku, Fukuoka 812-8582, Japan

[2] Department of Neurosurgery, Graduate School of Medicine, Kyushu University, 3-1-1 Maidashi, Higashiku, Fukuoka 812-8582, Japan

[3] Department of Bioengineering, National Cardiovascular Center Research Institute, 5-7-1 Fujishirodai, Suita, Osaka 565-8565, Japan

Received 3 June 2002; revised 7 November 2002; accepted 4 December 2002

Abstract: A novel photocurable tissue adhesive glue, which is composed of styrene-derivatized (styrenated) gelatin, poly(ethylene glycol) diacrylate (PEGDA), and carboxylated camphorquinone in phosphate-buffered saline (PBS), was prepared. The prototype formulation suitable for arterial repair was determined based on the gel yield, degree of swelling, tissue adhesive strength, and breaking (or burst) strength *in vitro*. The formulated photocurable tissue adhesive glue with an appropriate viscosity was converted to a water-swollen gel within 1 min of visible light irradiation. The tissue adhesive glue, which was coated on a rat abdominal aorta incised with a pair of scissors, was immediately converted to a swollen gel upon subsequent irradiation with visible light, and concomitantly hemostasis was completed. Histological examination showed that the produced gel was tightly adhered to the artery shortly after photoirradiation. The gel gradually degraded with time and was completely absorbed within 4 weeks after treatment. These results indicate that the photocurable glue developed here may serve as a tissue adhesive glue applicable to vascular surgery. © 2003 Wiley Periodicals, Inc. J Biomed Mater Res Part B: Appl Biomater 66B: 439–446, 2003

Keywords: photocurable tissue adhesive glue; styrene-derivatized gelatin; poly(ethylene glycol) diacrylate; visible light; photogelation

INTRODUCTION

In surgical operations, uncontrollable bleeding during surgery is often a life-or-death situation. The initial requirements for a tissue adhesive glue for soft tissue during a anastomosis or hemostasis process are as follows: rapid sol- or liquid-to-gel transformation, which should occur within a few minutes, strong adhesivity to wet natural tissues, and high burst strength, which provide protection against hydrodynamical pressure derived from bleeding, as well as physiological stresses such as pulsatile stress in arteries. In addition, such a tissue adhesive glue should interact with body defense mechanisms to induce thrombus formation. Furthermore, after the bleeding is completed, such a gel should be biodegraded and bioresorbed as the wound is healed.

A few synthetic and biologically derived tissue adhesive glues are currently available. Cyanoacrylate[1,2] and fibrin glue[1,3] are liquid glues, and absorbable gelatin sponge, oxidized regenerated cellulose, and microfibrillar collagen[4] are solid hemostatic aids. These glues have intrinsic advantages and disadvantages. For example, cyanoacrylate glue[2] exhibits very fast curing but becomes very brittle when cured and produces toxic substances when biodegraded. On the other hand, fibrin glue[3] is nontoxic in nature and has excellent wound-healing characteristics, but a major drawback is the very slow curing rate and weak mechanical properties of the cured glue. Thus, a reliable ideal tissue adhesive glue, which fully satisfies the requirements of rapid curing, flexibility, resistance to internal mechanical stress such as pulsating of soft tissue, little adverse tissue reaction, and reasonably rapid biodegradation, is still in great demand for surgery.

Correspondence to: Takehisa Matsuda, Department of Biomedical Engineering, Graduate School of Medicine, Kyushu University, 3-1-1 Maidashi, Higashiku, Fukuoka 812-8582, Japan (e-mail: matsuda@med.kyushu-u.ac.jp)

Contract grant sponsor: Promotion Fundamental Studies in Health Science of the Organization for Pharmaceutical Safety and Research (OPSR); contract grant number: 97-15

Contract grant sponsor: Ministry of Education, Culture, Sports, Science, and Technology of Japan; contract grant number: A2-12358017, B2-12470277

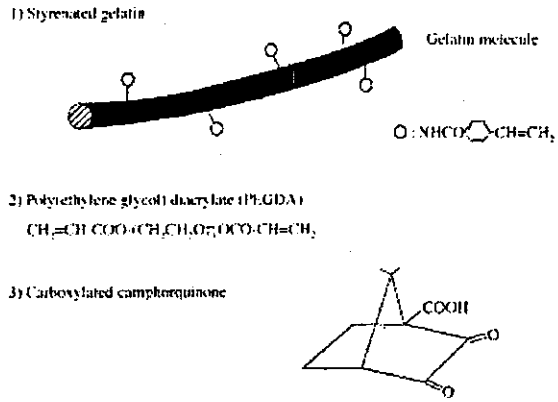

Figure 1. The chemical structure of ingredients of photocurable tissue adhesive glue.

A photoinduced wound-healing technology in which sol-to-gel transformation is driven by photochemical reactions is under development.[5–8] A previous study demonstrated an ultraviolet- (UV) light-curable glue in which a viscous buffer solution of poly(ethylene glycol) diacrylate (PEGDA) in the presence of a UV-induced radical generator multiply coupled to the gelatin molecules, was converted to a water-swellable gel upon UV irradiation.[7,8] This enables rapid gelation, hemostasis, and wound healing. However, major drawbacks of this system are as follows. UV-light irradiation is potentially harmful to living tissues. In addition, UV light does not penetrate into thick glue, so only surface-layer hardening or curing occurs. Relatively weak tissue adhesive strength derived from water-adsorptive characteristics of PEGDA did not allow protect against mechanical delamination from wet tissue surface.

On the other hand, Sawhney, Pathak, and Hubbell developed a visible-light-induced photopolymerizable glue based on hydrolytically degradable poly(ethylene glycol) diacrylate derivatives and visible-light-induced photoradical generator (eosin Y).[9] This rapidly curable glue is now being commercialized.

To overcome the shortcomings of the UV system and to achieve greater tissue adhesive strength, a new visible-light-induced photocurable tissue adhesive glue has been developed. The glue is a mixed buffer solution containing styrenated gelatin,[10] PEGDA and a carboxylated camphorquinone,[11] (1S)-7,7-dimethyl-2,3-dioxobicyclo[2.2.1]-heptane-1-carboxylic acid, as shown in Figure 1 (note that camphorquinone has been used as a radical generator for dental resins for curing for many years[19]). This photocurable glue is structured as an interpenetrating, as well as interconnecting, network of the copolymer of PEGDA and styrenated gelatin molecules. Previous studies[10–12] have shown that styrenated gelatin serves as a biodegradable, *in situ* gelable drug-releasing matrix, and coatings and scaffolds have potential use for tissue engineering. In this article, the authors attempted to develop a prototype tissue adhesive glue suitably formulated for arterial repair, which is determined in terms of the photocuring rate, gel yield, degree of swelling, and mechanical property of photocured gel (breaking strength and tissue adhesive strength). Very rapid hemostasis and biodegradability in the rat abdominal aorta model were demonstrated. The visible light-induced gelatinous glue may be suited for tissue adhesive of arteries in vascular surgery applications.

MATERIALS AND METHODS

Materials

Gelatin (molecular weight: 9.5×10^4 g/mol) and 0.1-N sodium hydroxide aqueous solution were obtained from Wako Pure Chemical Industry Ltd. (Osaka, Japan). 4-Vinyl benzoic acid was purchased from Tokyo Chemical Industry Co., Ltd. (Tokyo, Japan), and 1-ethyl-3-(3-dimethylaminopropyl)-carbodiimide hydrochloride as a water-soluble condensation agent (WSC) was purchased from Dojin Co. (Kumamoto, Japan). Phosphate-buffered saline (PBS) and 6-N hydrochloric acid aqueous solution were obtained from Katayama Chemical Co. (Osaka, Japan). Poly(ethylene glycol) diacrylate (PEGDA) with a molecular weight of 1000 g/mol was obtained from Polysciences, Inc. (Warrington, PA). A carboxylated camphorquinone (as shown in Figure 1) was prepared according to a previous method.[11] All other chemicals were of reagent grade and were used without further purification.

Preparation of Photocurable Glue

The preparation of styrenated gelatin is basically the same as in a previously reported method.[10] Briefly, 4-vinyl benzoic acid (11.4 g) was dissolved in 800 ml of an aqueous sodium hydroxide solution (0.1 N), and was then neutralized to about pH 7.5 with 6.0 N hydrochloric acid. Twenty grams of gelatin was dissolved in 1000 ml of PBS with stirring at 60 °C. These solutions were mixed and stirred for 30 min at 0 °C after WSC (29.6 g) was added, and then stirred overnight at room temperature. The reaction mixture was dialyzed with the use of a seamless cellulose tube (dialysis membrane, size 36, Viskase Co.) in deionized water for 3 days and then lyophilized with the use of a freeze dryer (FD-1, Tokyo Rikakikai Co. Ltd., Tokyo, Japan) under reduced pressure to obtain the styrene-derivatized gelatin (styrenated gelatin) in the form of a white powder. The number of styrene groups incorporated into a gelatin molecule was determined according to the method previously reported[6,8] using the trinitrobenzene sulfononic acid method and UV spectroscopy (DU series 500, Beckman, Tokyo, Japan). The degree of derivatization (approximately 33 styrene groups per molecule) was calculated based on the maximum number of amino residues available for derivatization (36.8 per molecule).

Photocurable glues were prepared by dissolution of the styrenated gelatin and 0.05 wt% carboxylated camphorquinone in PBS at 40 °C, with or without PEGDA. The solution obtained was centrifuged for 10 min for degassing and de-

bubbling. Figure 1 shows the chemical structure of ingredients of the photocurable glue.

Photoirradiation

Visible-light irradiation was conducted with the use of a Tokuso Power Lite (wavelength: 400–520 nm, 12 V-80 W, Tokuyama Co., Tokyo) through an optical fiber (diameter: 11 mm) at the intensity of 1.3×10^6 lx.

Determination of Gel Yield and Swellability

To determine the optimum formulation of the photocurable glue, gel yield and degree of swelling were selected as indices as follows. Onto a circular glass cover slip (diameter: 11 mm), 100 μl of the glue prewarmed to 37 °C (weight of the solid content: W_{solid}) was poured and then photoirradiated for a predetermined time. After repeated thorough extraction with hot distilled water to remove nonreacted substances, the disk-shaped gels obtained were allowed to equilibrate with water overnight at room temperature, and were then weighed (W_{water}) after excess water had been carefully swabbed. The vacuum-dried gels were weighed (W_{gel}). The gel yield (%) was calculated as $W_{gel}/W_{solid} \times 100$. The degree of swelling was calculated as $(W_{water} - W_{gel})/W_{gel}$. The experiments were repeated five times; only the average values are reported.

Mechanical Properties

The breaking strength of the photocured glues was measured with a rheometer (RE-3305, Yamaden Co., Tokyo) by an indentation technique. The system, equipped with a 3-mm-diameter rodlike Teflon probe and a sample stage having a 5-mm-diameter hole at its center, can be used to measure the amount of indentation by the probe into the gel as a function of the force applied. Water-swollen disk-shaped gels of about 1.5 mm in thickness, prepared by casting 200 μl of various photocurable glues on a circular glass cover slip (diameter: 11 mm) and subsequently photoirradiating for 1 min to ensure complete gelation, were fixed at the center of the sample stage of the rheometer. The force applied was recorded until rupture of the gels occurred due to continuous loading of tension to the center of the gels, using the probe at a rate of 0.5 mm/s in distilled water. The maximum stress (P), defined as breaking strength, was calculated as P (Pa) = A (g) $\times$ 980/10 $\times$ S(cm^2), where A and S denote the force at gel rupture and the contact area of the probe (0.07 cm^2), respectively.

The adhesive strength of the photocured glue was measured also with a rheometer. The glue was coated onto part (area: 0.5 cm^2) of a water-swollen collagen film (3 $\times$ 3 cm^2 collagen casing, Nippi Inc., Tokyo) and was then transformed into a gel by applying 1 min of photoirradiation. The gel produced was removed from the collagen in distilled water at a rate of 1 mm/s with the use of the above-mentioned rheometer, and the force applied until the gel and the collagen film separated was recorded. The maximum stress, obtained by conversion of the maximum force with the above-mentioned equation, was defined as the adhesive strength.

Hemostasis of Artery

Hemostasis studies were performed with the use of 6–7-week-old Wistar rats (average weight: 250 g). Rats were administered general anesthesia of diethyl ether and pentobarbital sodium (25 mg/kg). No anticoagulant was used. The abdominal aorta was surgically exposed and isolated by placing arterial clamps at a distance of about 1–2 cm. The isolated zone was mechanically incised (length: 2–4 mm) with a pair of scissors. The photocurable tissue adhesive (20 μl) was applied to the severed part and subsequently irradiated with visible light for 1 min. Then the clamps were removed to allow blood to flow again. The tissue adhesivity was evaluated from macroscopic observation whether bleeding occurred or not. Immediately after surgery, the injured segments of the harvested arteries were rinsed of blood. After the predetermined intervals of 1, 2, and 4 weeks, arteries with surrounding tissues were harvested, fixed with 20% formalin solution, embedded in paraffin, sectioned at a thickness of 6 μm, and dehydrated in a graded ethanol series. After staining with hematoxylin-eosin, artery specimens were evaluated by light microscopy. All animal studies were carried out according to the Principles of Laboratory Animal Care (formulated by the National Society for Medical Research) and the Guide for the Care and Use of Laboratory Animals (National Institutes of Health, Publication No. 85-23, revised 1985).

Statistical Analysis

Statistical analysis was performed with the StatView 5.0 program (Abacus, Berkley, CA). Data were shown as mean $\pm$ standard deviation (SD). The values were subjected to statistical analysis with the use of analysis of variance (ANOVA). Differences among the groups were assessed by the Tukey–Kramer post hoc test with the significance level at $p = 0.05$.

RESULTS

Determination of Prototype Formulation

Photocurable tissue adhesive glue under development was a buffer solution containing styrenated gelatin (in which approximately 33 styrene groups are incorporated in a gelatin molecule; molecular weight: 9.5×10^4 g/mol), poly(ethylene glycol) diacrylate (PEGDA, molecular weight: 1000 g/mol), and a carboxylated camphorquinone (Figure 1). The concentration of carboxylated camphorquinone as the initiator agent was fixed at 0.05 wt% in this experiment (note that a previous study indicated that the photocuring rate leveled off beyond this concentration).[12] The mixing of styrenated gelatin with PEGDA at relatively high concentrations of both ingredients (for example, 45 wt% of styrenated gelatin and 10 wt% of PEGDA) yielded a milky viscous solution, indicating that

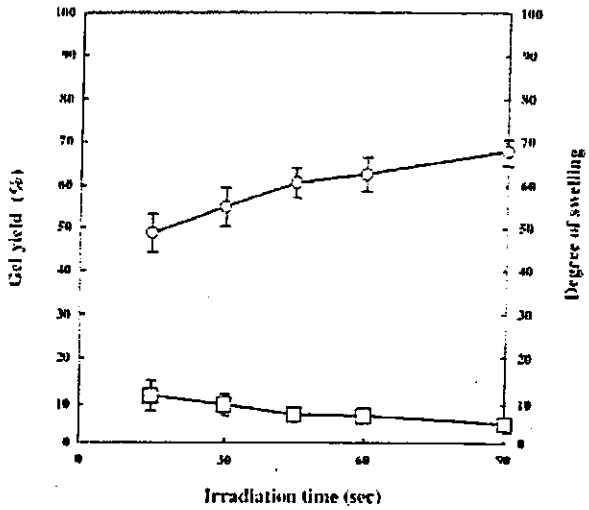

Figure 2. Relationship of gel yield (circles) and the degree of swelling (squares) with irradiation time for a mixture with 35 wt% of styrenated gelatin and 5 wt% of PEGDA. CQ concentration was fixed at 0.05 wt%. Photointensity was fixed at 1.3×10^6 lx. Experiments were repeated five times independently. The data are expressed as means ± SD.

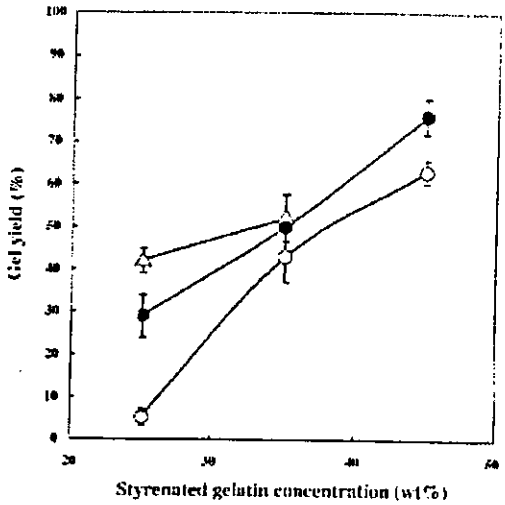

Figure 3. Relationship of the gel yield with styrenated gelatin concentration. CQ concentration was fixed at 0.05 wt%. Photoirradiation time and intensity were fixed at 1 min and 1.3×10^6 lx, respectively. The PEGDA concentrations were 0 (open circles), 5 wt% (solid circles), and 10 wt% (triangles). Experiments were repeated five times independently. The data are expressed as means ± SD.

these two ingredients did not mix well at this concentration, which eventually separated into two phases when left to stand. However, no phase separation occurred below these concentrations.

First, the photoirradiation time dependence on gel yield was assessed prior to a prototype formulation for *in situ* gelable tissue adhesive. Figure 2 shows the photoirradiation-time dependence of gel yield and degree of swelling for the glue composed of 35 wt% of styrenated gelatin with 5 wt% of PEGDA. Very rapid gelation occurred within 15 s of irradiation at an intensity of 1.3×10^6 lx, followed by a gradual increase in the gel yield with photoirradiation time and gradual decrease in the degree of swelling. After 45 s of irradiation, although gel yield increased slightly and degree of swelling decreased slightly even upon prolonged irradiation, both parameters appeared to be loaded off. Therefore, the photoirradiation time was fixed at 1 min thereafter.

Figure 3 shows the gel yield dependence on the concentration of styrenated gelatin with or without PEGDA under fixed photoirradiation conditions (irradiation time, 1 min, photointensity, 1.3×10^6 lx). At a low styrenated gelatin concentration, a marked difference in photogelation characteristics or gel yield was noticed: the higher the PEGDA concentration, the higher the gel yield is. The gel yield increased with increasing concentration of styrenated gelatin, but the PEGDA concentration dependence on gel yield decreased at high styrenated gelatin concentration.

The degree of swelling of the photocured gel for various compositions of mixed solutions with up to 45 wt% of styrenated gelatin is shown in Figure 4. At a low styrenated gelatin concentration, a very high swelling was noticed for non-PEGDA containing styrenated gelatin. The increase in PEGDA concentration tended to lower the degree of swelling. The degree of swelling decreased with increasing concentrations of styrenated gelatin and PEGDA. At 45 wt% of styrenated gelatin, the degree of swelling became minimal, approximately 3–5 regardless of concentration of PEGDA.

Figure 5 shows the breaking strength of photoproduced gels, determined by the indentation technique, which may simulate hydrodynamic pressure-induced inflation of gel. The higher the breaking strength, more durable the glue is. The

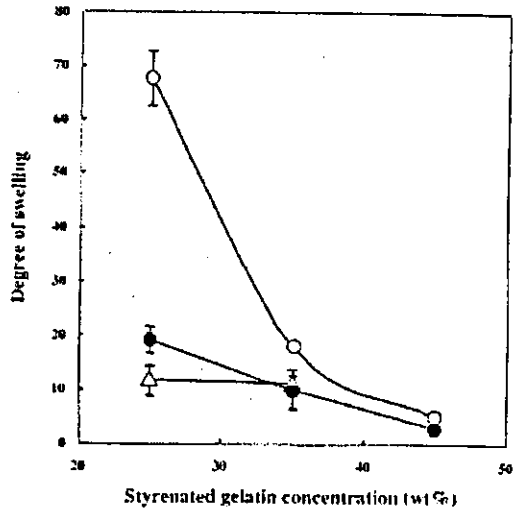

Figure 4. Relationship of the degree of swelling with styrenated gelatin concentration. CQ concentration was fixed at 0.05 wt%. Photoirradiation time and intensity were fixed at 1 min and 1.3×10^6 lx, respectively. The PEGDA concentrations were 0 (open circles), 5 wt% (solid circles), and 10 wt% (triangles). Experiments were repeated five times independently. The data are expressed as means ± SD.

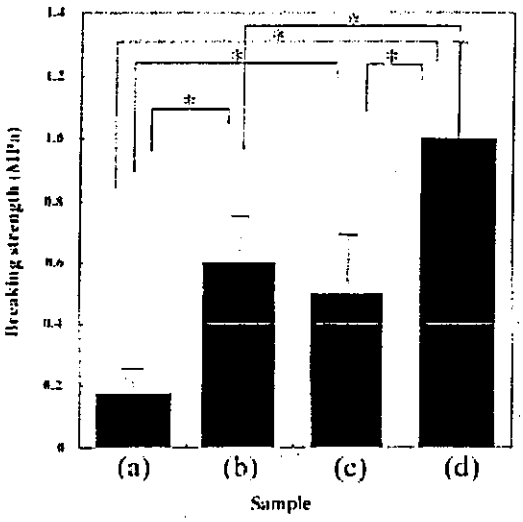

Figure 5. Breaking strength of photoproduced gel. The samples contained (a) 35 wt% of styrenated gelatin , (b) 35 wt% of styrenated gelatin with 5 wt% of PEGDA, (c) 35 wt% of styrenated gelatin with 10 wt% of PEGDA, and (d) 45 wt% of styrenated gelatin with 5 wt% of PEGDA. CQ concentration was fixed at 0.05 wt%. Photoirradiation time and intensity were fixed at 1 min and 1.3×10^6 lx, respectively. Experiments were repeated five times independently. The data using Fisher's test are expressed as means ± SD. *Significant at $p < 0.05$

calculated breaking strengths were as follows: 0.18 MPa for 35 wt% of styrenated gelatin, 0.60 MPa for 35 wt% of styrenated gelatin/5 wt% of PEGDA mixture, 0.50 MPa for 35 wt% of styrenated gelatin/10 wt% of PEGDA mixture, and 1.04 MPa for 45 wt% of styrenated gelatin/5 wt% of the PEGDA mixture.

Figure 6 shows the adhesive strength of gels which were photoproduced on wet collagen films, which may simulate mechanical failure due to shear stress-induced delamination. For a 35 wt% styrenated gelatin mixed with or without 5 wt% PEGDA, high strength appeared to be achieved with a styrenated gelatin concentration of 35 wt%. For the gels with 35 wt% styrenated gelatin premixed with PEGDA, the adhesive strength progressively decreased with an increase in the PEGDA concentration.

Based on these results, the following conclusion may be drawn: At a low styrenated gelatin concentration (25 wt%), a very low gel yield and a very high degree of swelling were noticed for a glue without PEGDA additive, indicating that such a photocured gel has very low mechanical integrity. An increase in styrenated gelatin concentration increased the gel yield and markedly reduced the degree of swelling (Figure 4). PEGDA additive increased the gel yield (Figures 2 and 3) and reduced the degree of swelling, and increased the breaking strength but reduced the adhesive strength to a wet collagen film (Figure 6). Although increasing the styrenated gelatin concentration to 45 wt% increased the gel yield and reduced the degree of swelling (Figures 3 and 4), a very high viscosity of the glue solution is a major drawback. Therefore, a prototype glue formulation for *in vivo* study was designed to be 35 wt% of styrenated gelatin and 5 wt% of PEGDA.

In Vivo Application and Degradation

Abdominal aorta (external diameter: approximately 2 mm) from Wistar rats, surgically exposed and isolated by placing arterial clamps at a distance of about 1–2 cm, were mechanically incised with a pair of scissors for 2–4 mm in the longitudinal direction [Figure 7(a)]. The bleeding from the incision was confirmed by declamping on the distal side. A small amount of the photocurable tissue adhesive glue (20 μl, 35 wt% of the styrenated gelatin and 5 wt% of PEGDA) was thoroughly coated onto the incised part without sagging. The glue was irradiated with visible light for 1 min, and then the clamp was removed to allow blood to flow again. The photocured gel exhibited very good tissue adhesivity without any bleeding [Figure 7(b)]. No delamination of the photocured gel layer occurred even after thorough washing with a saline solution. In addition, the adhesive-applied anastomosed vessels could pulsate synchronously with blood pressure, which would cause little disturbance of downstream pulsation in vascular systems. On the other hand, when a solution containing 35 wt% of styrenated gelatin without PEGDA was applied, a photocured gelatin was often inflated partially to create a thinner gel layer, and sooner or later rupture occurred, resulting in bleeding. This may be due to low breaking strength, as shown in Figure 5. The summary of acute phase tissue adhesive gluing is as follows: neither bleeding nor inflation and delamination was observed for styrenated gelatin/PEGDA mixed system ($n = 45$), whereas bleeding occurred in one third of trials but no delamination was observed for only styrenated gelatin ($n = 32$). Thus, the addition of PEGDA strengthened durability of tissue adhesive glue without appreciable loss of adhesivity.

The *in vivo* degradation of the photocurable tissue adhesive glue and wound healing were evaluated through a histological examination of the rat abdominal aorta wound model described above. Micrographs of the cross sections of incised aorta coated with photocured gels after 1, 2, and 4 weeks of treatment are shown in Figure 8. Immediately after photoirradiation of the tissue adhesive glue, photocured gel

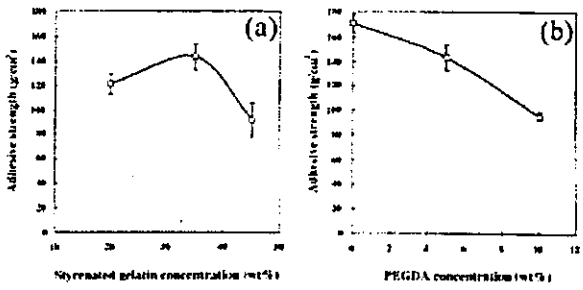

Figure 6. Adhesive strength to collagen film. (a) Relationship of adhesive strength withstyrenated gelatin concentration mixed with 5 wt% of PEGDA. (b) Relationship of adhesive strength with PEGDA concentration mixed with 35 wt% of styrenated gelatin. CQ concentration was fixed at 0.05 wt%. Photoirradiation time and intensity were fixed at 1 min and 1.3×10^6 lx, respectively. Experiments were repeated five times independently. The data are expressed as means ± SD.

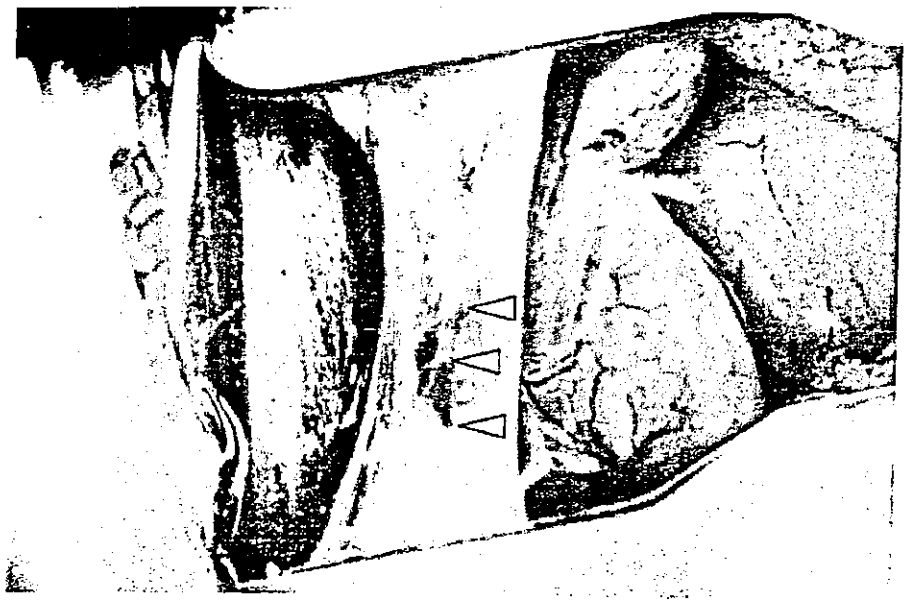

(a)

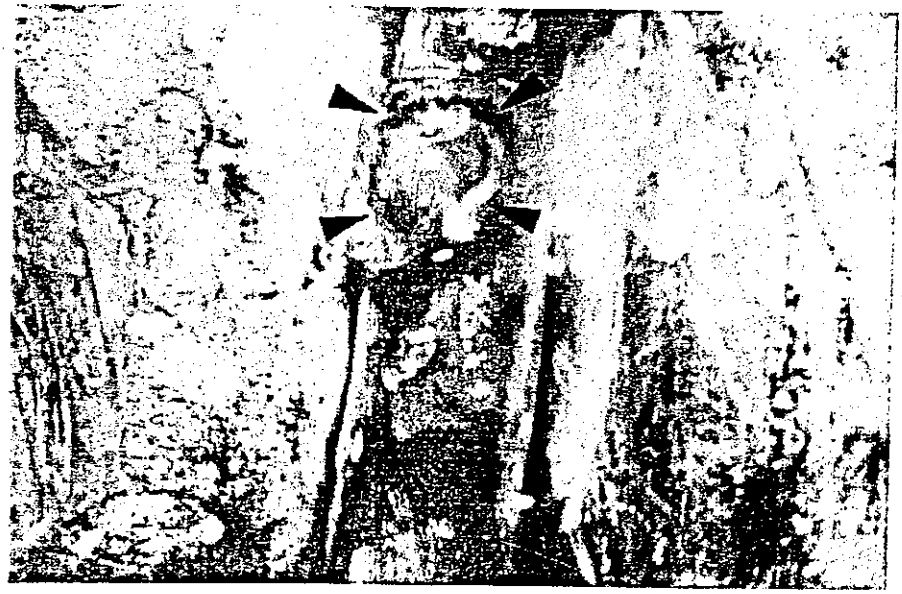

(b)

Figure 7. Anastomosis of rat abdominal aorta using the photocurable tissue adhesive glue. (a) Rat abdominal aorta mechanically incised in longitudinal direction. (b) Abdominal aorta irradiated with visible light after coating with 20 μl of the photocurable tissue adhesive glue (35 wt% of styrenated gelatin and 5 wt% of PEGDA). White arrowhead: wound. Solid arrowhead: photoproduced gel.

completely filled the artery wound. None of the treated rats died within the projected sacrifice periods of up to 4 weeks after surgery. No cellular infiltration occurred inside the gel or wound [Figure 8(a)]. One week after surgery, the injured tissue site was not yet repaired and the acute inflammatory reaction was dominated by the foreign-body process. Fragments of the gel were encapsulated by a large number of cells, probably inflammation-related cells [Figure 8(b)]. Two weeks after surgery, massive cell accumulation was noted at the wound site; fibroblast-like cells had accumulated around the wound. The gel was degraded into small pieces, which were encapsulated [Figure 8(c)]. At 4 weeks after surgery, fibroblast-like cells existed around the wound, but the number of cells was considerably reduced. The gel had completely disappeared at this time [Figure 8(d)]. New tissue was regenerated without excessive thickening.

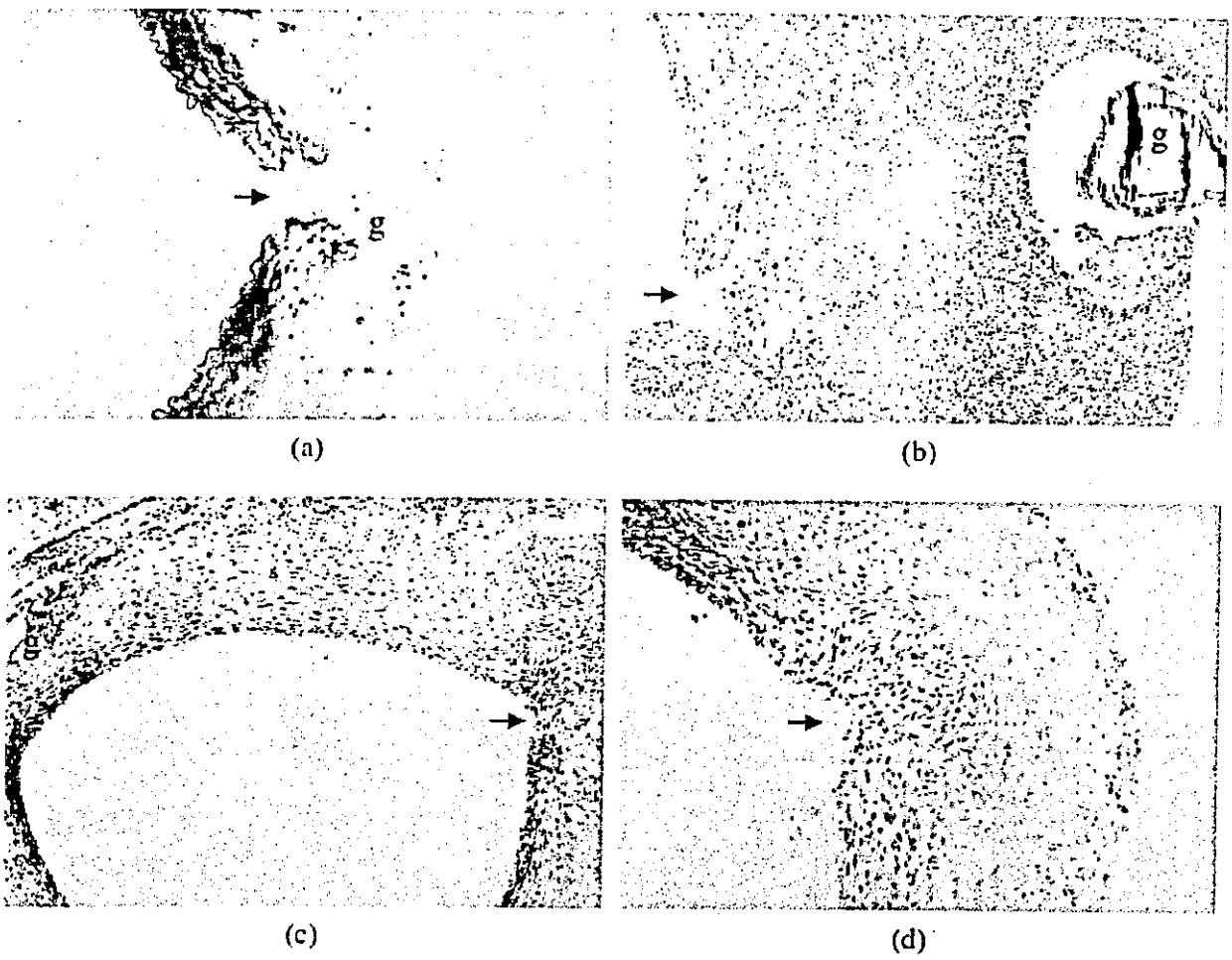

Figure 8. Biodegradation of photocurable tissue adhesive glue. Histological micrographs of the rat abdominal aorta: (a) immediately after irradiation; (b) 1 week after surgery; (c) 2 weeks after surgery; (d) 4 weeks after surgery. Hematoxylin-eosin stain, magnification × 100. g: Photocured tissue adhesive glue. Arrow: wound.

DISCUSSION

The major requirements of a topical tissue adhesive glue are rapid gelation, which should be completed within 1 min, strong tissue adhesivity to natural wet tissue, and durability to hostile mechanical stress environments. That is, withstanding hydrodynamic pressure due to bleeding, as well as physiological stresses such as pulsatile stress in arteries, is essential. In addition, a tissue adhesive glue should trigger thrombus formation but minimize the activation of other body defense mechanisms. Furthermore, after hemostasis, such a gel should be biodegraded and bioresorbed in concert with wound-healing action.

The authors previously studied a UV-light-irradiation-induced photocuring system composed of UV-sensitive group-derivatized gelatin and PEGDA.[7,8] However, avoiding potential hazards such as cellular damage due to UV light irradiation was the most critical task. In this study, in order to satisfy the requirements described above while minimizing such potential damage, a novel visible-light-induced hemostatic coating system was designed based on visible-light-induced photo-copolymerization of multiply derivatized styrenated gelatin and PEGDA. Irradiation of visible light onto the tissue adhesive glue produced a gel with a wide range of mechanical and physiochemical properties from very soft and highly swollen to relatively rigid and minimally swollen, depending on the formulation variables and photoirradiation conditions. The gelation occurs due to the intra- and intermolecular copolymerizations of the styrene group and of styrenated gelatin acrylate group of PEGDA.

Gelation characteristics such as gelation time, gel yield, breaking (or burst) strength, and tissue adhesive strength are controlled by many factors such as the material used, formulation, and operation factors. A multifactorial design was carried out for the structure–performance relationships in terms of gelation rate, gel yield, gel swelling, and viscosity, all of which are dependent on degree of styrene derivatization in gelatin molecule, concentrations of styrenated gelatin and camphorquinone, photointensity, and irradiation time.

A formulation of 35 wt% of styrenated gelatin (approximately 89% of the lysine group is styrenated: approximately 33 styrene groups per gelatin molecule), 5 wt% of PEGDA, and 0.05 wt% of carboxylated camphorquinone in PBS was selected. This formulation appears to provide reasonably short gelation time (curing with 1 min irradiation), relatively high gel yield (Figures 2 and 3), reduced degree of swelling (Figure 4), high burst strength (Figure 5), and high tissue adhesivity (Figure 6). In addition, an applied viscosity of designed tissue adhesive glue was appropriate, which permits complete coating on vascular tissues without sagging.

Animal studies using rat abdominal aorta confirmed that the viscous tissue adhesive glue was immediately converted to a swollen gel upon 1 min of photoirradiation with little tissue damage, resulting in complete hemostasis. The formed gels adhered well to wet surfaces and appeared to be able to deform in response to artery movement [Figure 7(b)]. Acute inflammatory reactions and fragmentation of gel were observed 1 week after surgery. This suggests that the inflammatory reaction and biodegradation proceeded well in this period. The photocurable hemostatic glue appeared to exhibit a high biodegradation rate. This biodegradation and bioabsorption progressed with time. Four weeks after surgery, the gel was completely absorbed, inflammatory cells had completely disappeared, and a few cells, probably fibroblasts around the wound, were observed. Although the authors did not identify the type of cells participating in tissue repair and foreign body reaction, tissue repair and biodegradation appear to proceed via normal tissue reactions.

Gelatin is nontoxic in nature,[13,14] induces cell adhesion via biospecific interaction,[15] and has been extensively used in biomedical applications, including hemostatic aid materials,[16,17] and cell adhesive matrices.[18] On the other hand, gelatin partially derivatized with 4-vinyl benzoic acid is a core material in ongoing wound-healing technology and tissue engineering. The preparation and purification of the styrenated gelatin are simple and reproducible. Such photocurable gelatin in combination of PEGDA appears to satisfy the requirements of a tissue adhesive glue in a high-pressure circulatory system, and may have a great potential for use in vascular surgery.

REFERENCES

1. Lerner R, Binur N. Current status of surgical adhesives. J Surg Res 1990;48:165–181.
2. Tseng YC, Tabata Y, Hyon SH, Ikada Y. *In vitro* toxicity test of 2-cyanoacrylate polymers by cell culture method. J Biomed Mater Res 1990;24:1355–1367.
3. Flahiff C, Feldman D, Salts R, Huang S. Mechanical properties of fibrin adhesives for blood vessel anastomosis. J Biomed Mater Res 1992;26:481–491.
4. Arand AG, Sawaya R. Intraoperative chemical hemostasis in neurosurgery. Neurosurgery 1986;18:223–233.
5. Matsuda T, Moghaddam MJ, Miwa H, Sakurai K, Iida F. Photoinduced prevention of tissue adhesion. ASAIO J 38:154–157;1992.
6. Nakayama Y, Matsuda T. Newly designed hemostatic technology based on photocurable gelatin. ASAIO J 1995;374–378.
7. Nakayama Y, Sakaguchi Y, Masuda S, Okano T, Matsuda T. Design of photocurable tissue adhesive consisting of photoreactive gelatin and poly(ethylene glycol) diacrylate: application for arterial surgery. Jpn J Artif Organs 1997;26:225–231.
8. Nakayama Y, Matsuda T. Photocurable surgical tissue adhesive glues composed of photoreactive gelatin and poly(ethylene glycol) diacrylate. J Biomed Mater Res Appl Biomater 1999;48: 511–521.
9. Sawhney AS, Pathak CP, Hubbell JA. Bioerodible hydrogels based on photopolymerized poly(ethylene glycol)-co-poly(α-hydroxy acid) diacrylate macromers. Macromol 1993;26:581–587.
10. Matsuda T, Magoshi T. Preparation of vinylated polysaccharides and photofabrication of tubular scaffolds as potential use in tissue engineering. Biomacromolecules 2002;3: 942–950.
11. Magoshi T, Matsuda T. Formation of polymerized mixed heparin/albumin surface layer and cellular adhesional responses. Biomacromolecules 2002;3:976–983.
12. Okino H, Nakayama Y, Tanaka M, Matsuda T. *In situ* hydrogelation of photocurable gelatin and drug release. J Biomed Mater Res 2002;59:233–245.
13. Clark DP, Hanke CW, Swanson NA. Dermal implants: Safety of products injected for soft tissue augmentation. J Am Acad Dermatol 1989;21:992–998.
14. Hastings GW. Polymer in medicine. Chem Br 1971;7:119–120.
15. Kreis T, Vale R, editors. Guidebook to the extracellular matrix and adhesion proteins. Oxford: Oxford University Press; 1993.
16. Otani Y, Tabata Y, Ikada Y. A new biological glue from gelatin and poly(L-glutamic acid). J Biomed Mater Res 1996;31:158–166.
17. Koehnlein HE, Lemperle G. Experimental studies with a new gelatin-resorcin-formaldehyde glue. Surgery 1969;66:377–382.
18. Fujimoto R, Nakayama Y, Matsuda T, Hara Y, Saishin M. Development of hybrid keratoprosthesis (4): Hybrid corneal tissue with mechanical compatibility and controlled cell adhesivity. Folia Ophthalomol Jpn 1995;46:357–364.
19. Fujimori Y, Kaneko T, Nishide H, Tsuchida E. Photoreaction and photoinitiation behavior in the light-cured dental resins. Koubunshi Ronbunshu 1993;50:485.

Connective Tissue Research, 44(Suppl. 1): 318–325, 2003

0300-8207/03 $12.00 + .00
DOI: 10.1080/03008200390181843

Taylor & Francis
healthsciences

Laser-Perforated Membranous Biomaterials Induced Pore Size-Dependent Bone Induction When Used as a New BMP Carrier

Y. Kuboki,[1,4] M. Kikuchi,[1] H. Takita,[1] R. Yoshimoto,[1] Y. Nakayama,[2] T. Matsuda,[2] and Y. Ikada[3]

[1]*Graduate School of Dental Medicine, Hokkaido University, Sapporo, Japan*
[2]*National Cardiovascular Center Research Institute, Osaka, Japan*
[3]*Institute for Frontier Medical Sciences, Kyoto University, Kyoto, Japan*
[4]*Koken Bioscience Institute, Tokyo, Japan*

Previously we found that laser perforation of a collagen membrane (35 μm thickness, Koken Co., Tokyo) produced an effective bone morphogenetic protein (BMP) carrier, if the created pore sizes were larger than 0.5 mm. In this study we applied the same technique to create pores of 0.2 and 1.0 mm in a thicker (1.2 mm thickness) porous biodegradable membrane made of polylactic acid and an ε-caprolactone copolymer (PLA-CL) to obtain an effective membranous BMP carrier with higher mechanical strength. Pieces of PLA-CL (0.5 × 1.0 × 0.12 cm) combined with rhBMP-2 (5 μg) were implanted subcutaneously into rats and processed for analyses at 1–3 weeks. The laser-perforated PLA-CL membranes equipped with 1.0 mm pores induced mineralization beginning from the margins of the pores judging from the X-ray patterns, but bone formation seemed to proceed irregularly inside the pores. In the perforated PLA-CL membrane with 1.0-mm pores bone formation did not significantly increase compared with the nonperforated one. This was due to the fact that the PLA-CL membrane was already a porous structure (85% porosity). In contrast with laser-perforated PLA-CL 0.2 mm pores, bone was induced on the collagen fibers and fiber bundles inside the pores. The different patterns of bone formation between the PLA-CL membranes with 1.0 and 0.2 mm pores seemed to be related to the active formation of perpendicular collagen fibers through the 0.2 mm pores.

Keywords Artificial ECM, BMP, Geometry, Laser Perforation, Osteogenesis.

Received 9 November 2001; accepted 2 March 2002.
Address correspondence to Yoshinori Kuboki, Department of Oral Health Science, Graduate School of Dental Medicine, Hokkaido University, N-13 W-7 Kita-Ku, Sapporo, 060-8586, Japan. E-mail: kuboki@den.hokudai.ac.jp

INTRODUCTION

To reconstruct the periodontal ligament and cementum, partially or de novo by tissue engineering, certain principles must be applied. In this regard, we have proposed that five factors must be considered [1–8]:

1. Cells directly involved in bone formation.
2. Matrices produced by the cells.
3. Body fluid provided by vascularization.
4. Regulators of general cellular activities as well as the calcification process.
5. Biomechanical dynamics.

Detailed analysis of each of these five factors, as well as of the interrelationships between them, and integration into the whole picture of tissue formation is an efficient way to achieve the purpose. To verify the above proposition, we chose as our experimental system bone morphogenetic protein (BMP)-induced ectopic osteogenesis [1–8]. BMP needs certain exogenous carriers to express its function of tissue induction in vivo [9]. Thus, we have developed and tested more than 10 biomaterials as BMP carriers and found that the BMP-induced tissue formation is highly dependent upon the carrier. It is now understood that the carrier of BMP functions not only as a mere drug delivery system, but also as an important cell substratum on which the cells undergo growth and differentiation. In this experimental system, BMP and its carriers corresponded to regulator and artificial matrices, respectively.

As far as matrices are concerned, their functions and properties are now being reconsidered from a new aspect, in which the geometrical factor is emphasized in addition to three other traditional factors; physical, chemical, and biochemical factors [1, 2]. For periodontal regeneration, a BMP carrier with a

membranous shape is assumed to be more advantageous than the particle or block forms, considering the tissue regeneration surrounding the root of the tooth. Nevertheless, only a few trials have been reported on periodontal regeneration using membranous biomaterials as the BMP carrier. Previously, we succeeded in regeneration of periodontal ligament, including the perpendicular collagen fibers and new cementum, in furcation defects in the monkey by means of a BMP and double-layer system using fibrous collagen membrane (FCM) [10]. However, as an experimental system, the furcation defect was rather limited in area, and probably the most feasible system for periodontal regeneration. If we attempt the extended periodontal regeneration, a membranous BMP carrier of higher mechanical strength than FCM will be necessary [11].

The new idea of controlling the porosity of the membranous BMP carrier with a laser beam was first introduced by our group using thin collagen film [4]. The perforated collagen film induced bone effectively if the perforated pore sizes were larger than 0.5 mm. But the collagen films were too thin and fragile in some cases. In the present study, laser perforation technology was further applied to a synthetic biodegradable membrane made of a polylactic acid-ε-caprolactone copolymer (PLA-CL), which was shown to be mechanically stronger than FCM and more elastic than polylactic acid [12].

MATERIALS AND METHODS

Laser Perforation of Collagen Film and PLA-CL Membrane

Membranes of the PLA-CL copolymer were prepared as reported previously [11]. Briefly, PLA-CL copolymer was synthesized by polymerization of DL-lactide and ε-caprolactone at 190°C for 5 hr in vacuo using stannous octoate as a catalyst. The copolymers were cast on a glass plate into a sponge-type membrane (1.2 mm in thickness) by means of the salt-leaking method. They were dried under reduced pressure at 45°C.

To obtain larger pores of 0.2 and 1.0 mm in diameter in the PLA-CL membrane, a carbon dioxide laser cutting apparatus (laser wavelength 10.6 μm, power 25 W, LC-8120, Nihon Denshi Kagaku, Kyoto, Japan) was used [13]. In the PLA-CL membranes, a ring-shaped perforation, in which the diameters of outer circles and inner circles were 0.6 and 0.2 mm, respectively (Figure 1C), was attempted in addition to regular circle-type perforation.

The shapes and arrangements of pores were precisely controlled by a computer system. The centers of the each circle were placed on the angle of a squire and geometrical homology was obtained by keeping a constant ratio (2:8) of perforated to nonperforated areas of the membrane in all perforation cases, as in the method already reported [4] (Figure 1D).

Implantation and Evaluation of Carriers

The laser-perforated PLA-CL membranes with pores 0.2 and 1.0 mm in diameter were each combined with 5 μg of rhBMP-2 (a kind gift from Yamanouchi Co., Japan), implanted subcutaneously into rats, and analyzed after being extracted at 1–3 weeks, according to the methods reported previously [3–5].

The effects of the laser-perforated collagen film and PLA-CL membrane as BMP carriers were tested by histological observation after decalcifying the implants in Blank-Rychlo solution at 4°C for 5 hr. In some specimens histological observation was done before decalcification to clarify that mineralization occurred. The implants were analyzed for calcium contents and alkaline phosphatase activity by the methods reported [3–5].

RESULTS

Morphology of the Laser-Perforated Product

Perforation of the collagen film and PLA-CL membrane by the laser beam was precisely performed as expected without damaging the remaining areas for both 1.0 mm (Figure 1A) and 0.2 mm (Figure 1B, 1D) pores, except for slight melting of materials on the inner surfaces of pores, which gave a smoother appearance than in other parts as seen in the scanning electron microscopy pattern (Figure 1A, 1B). In the ring-type perforation (Figure 1C), it could be seen that the inner circle was partially attached via bridges to the inner surfaces of the pores.

Morphological and Biochemical Observations

In Figure 2, time-dependent changes in X-ray photographic profile of the PLA-CL with and without pores (1.0 mm) were shown. In the perforated groups (upper lanes in Figure 2A–2C), mineralization seemed to start from the margins of the pores at 2 weeks and extended to other areas at 3 weeks. In the nonperforated groups (lower lanes in Figure 3A–3C), mineralization was not clear at 2 weeks but becomes conspicuous at 3 weeks. These changes were consistent with the analysis of the calcium contents (Figure 4A).

Histological observations (Figure 3) indicated that PLA-CL membranes (1.2 mm thickness) with pores 1.0 or 0.2 mm in diameter induced bone formation started at 2 weeks (Figure 3A, 3C), following chondrogenesis (Figure 3B) at 1 week. At 3 weeks in the pore 1.0 mm bone formation became conspicuous and occupied most of pore space as shown in Figure 3E in an undecalcified section.

These laser-perforated PLA-CL membranes with the pore 0.2 or 1.0 mm did not show the clear concentric pattern of bone formation, unlike the X-ray patterns of mineralization along the margins of the pore. Rather, the membrane with the pore 1.0 mm formed irregular pattern of bone insides the pores (Figure 3A, 3F). Cartilage formation was often observed at 1 week after implantation in both PLA-CL membranes (Figure 3B), which was in contrast to the results obtained for the laser-perforated collagen films, in that we could not detect any cartilage in the perforated membrane with any pore size [4]. Bone formation was observed in the nonperforated membranes within the small fissures and holes, which was also seen in the nonperforated areas in the perforated PLA-CL membrane (Figure 3F). The perforated PLA-CL membranes implanted without rhBMP-2 did not

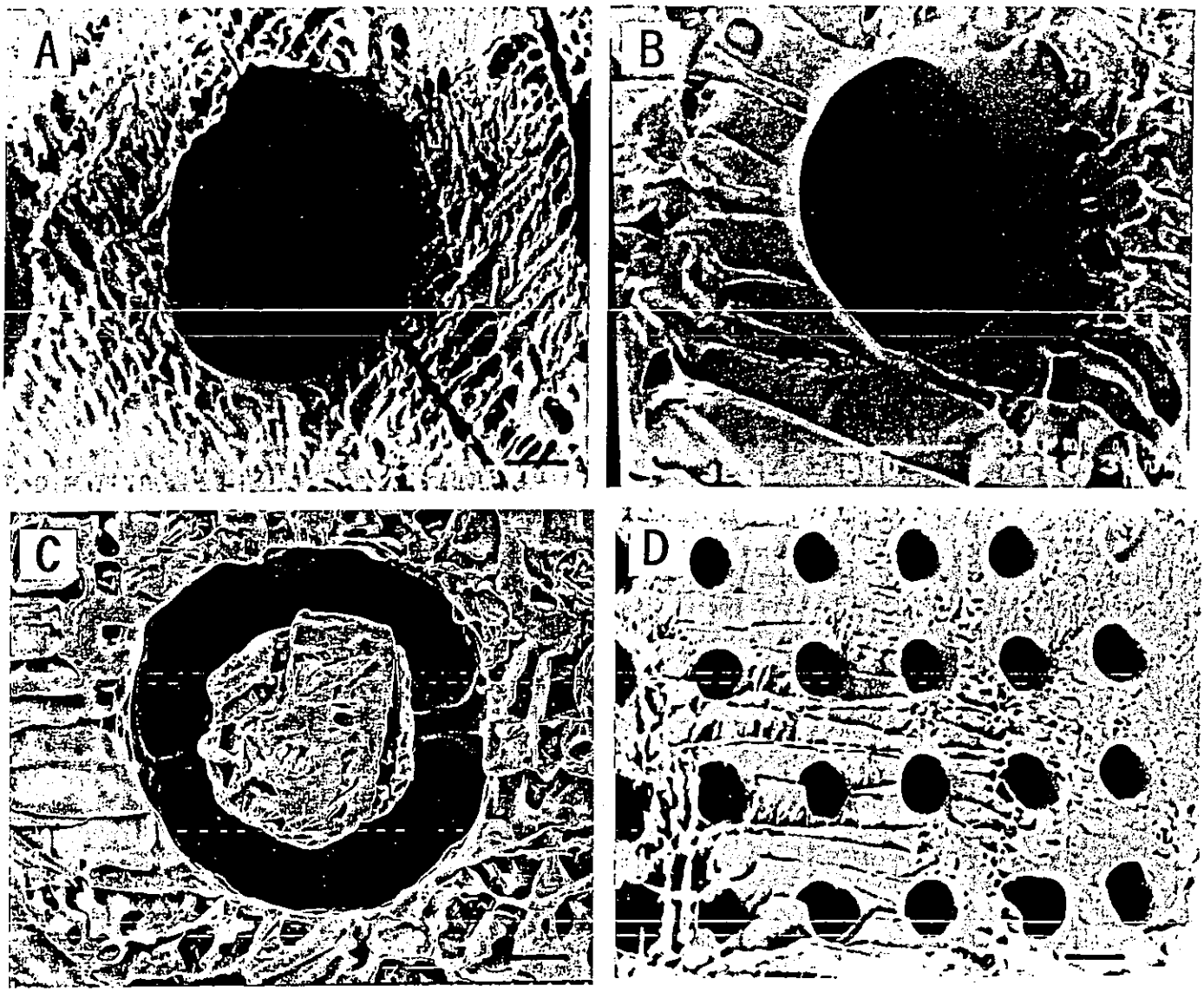

Figure 1. Scanning electron microscopy profiles of the laser perforated PLA-CL membranes. Porous structures other than the laser-perforated pores are observed. These include numerous fissures and holes, inside and on the surfaces of the membrane. (A) PLA-CL membrane with pores 1.0 mm in diameter, (B) membrane with pores 0.2 mm in diameter, (C) the ring-type pores with outer and inner diameters of 1.0 and 0.6 mm, respectively, and (D) pores of 0.2 mm in a lower magnification. Solid bars indicate 0.2 mm.

induce bone or cartilage. Generally, loose fibrous connectives occupied the pores irregularly.

In the biochemical parameters of calcium contents and alkaline phosphatase activity as shown in Figure 4A and 4B, we could not find a significant difference between the perforated groups and the nonperforated one. However, we could see a tendency of time-dependent increases in calcium contents and alkaline phosphatase activities in both perforated and nonperforated PLA-CL membranes. Statistical difference was clear between calcium contents of nonperforated PLA-CL at 1 and 3 weeks ($p < .05$). Calcium content at 3 weeks (0.6–1.0 mg) was slightly lower than the results from the perforated collagen films (1.2–1.4 mg per carrier) under very similar experimental conditions [4]. However, these values were much lower than that of the most efficient BMP carrier, insoluble bone matrix, which exhibits more than 5 mg calcium per carrier when implanted with 5 μg of rhBMP-2 [15].

Perpendicular Development of Collagen Fibers

It was remarkable that collagen fibers and fiber bundles ran perpendicularly to the membrane in the PLA-CL membrane with pores of 0.2 mm (Figure 3D) and in the ring-typed pores with 0.2 mm ring width (Figure 3C). On the other hand, in the 1.0 mm pores, fibers were random in orientation, running perpendicularly only in the surface of the carrier, but horizontally

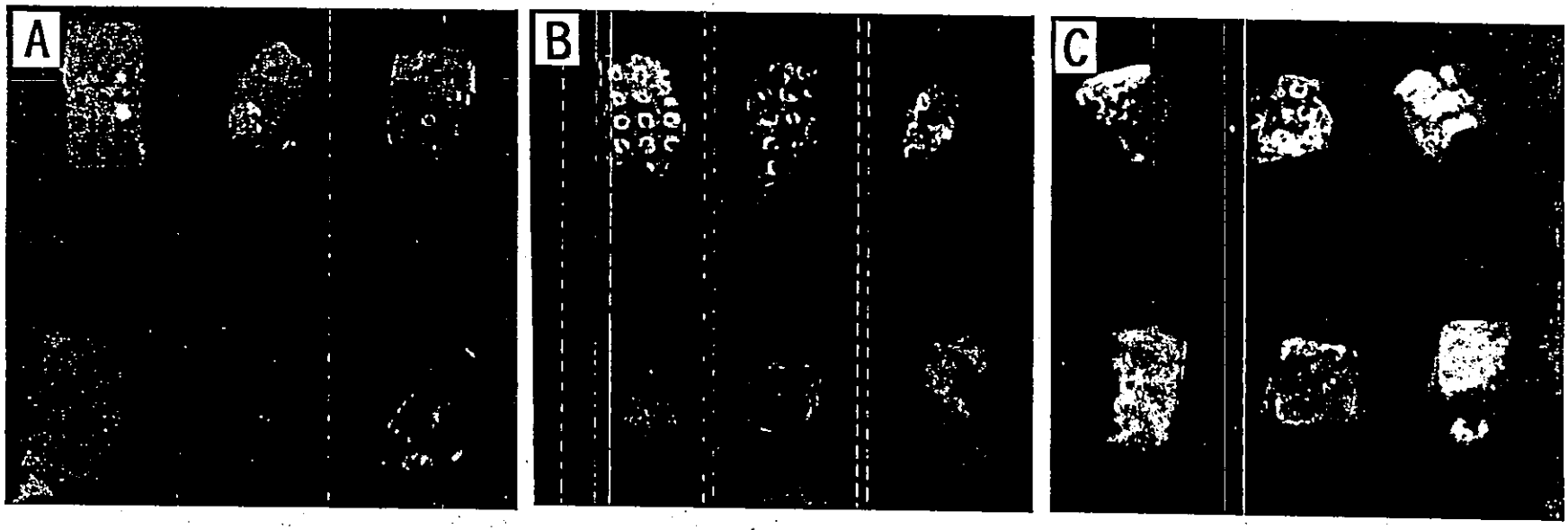

Figure 2. Time-dependent change in soft X-ray photographic profile of the PLA-CL membranes with and without pores (1.0 mm) implanted with rhBMP-2. In the perforated groups (upper lanes), mineralization started from the margins of the pores at 2 weeks and extended to other areas at 3 weeks. In the nonperforated group (lower lanes), mineralization was not clear at 2 weeks but becomes conspicuous at 3 weeks. These changes were consistent with the analysis of the calcium contents (Figure 4A). Figures A, B, and C indicate the extracted samples at 1, 2, and 3 weeks.

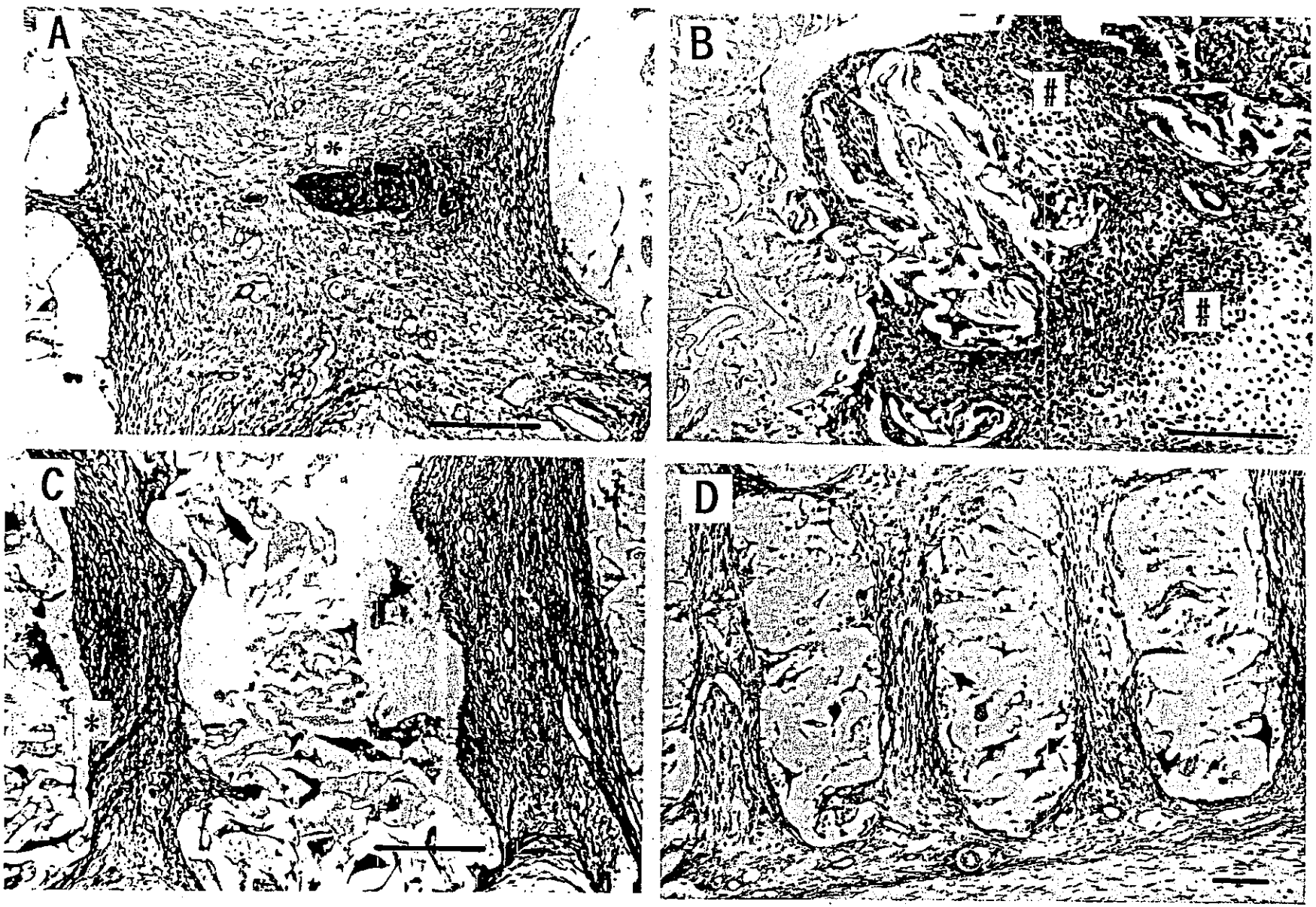

Figure 3. Histological observations of the PLA-CL membranes with the pores 1.0 mm (A, B, and E) and 0.2 mm (C, D, and F) implanted with rhBMP-2. In the 1.0 mm pores, bone formation started inside the pores, not directly on the carrier surface at 2 weeks (* in A), and cartilage formation was seen at 1 week (# in B). At 3 weeks, bone formation in the 1.0 mm pores became more conspicuous (E) in an undecalcified section. In the ring-type pores with 0.2 mm ring width (C) and the open pores 0.2 mm (D), actively orientated development of collagen fibers was characteristic, and bone formation occurred along the collagenous matrices (* in C) at 2 weeks. Bone formation in the 0.2 mm pores was clearly seen in cross-section at 2 weeks (F). Figures A, C, D, and E are in a vertical section to the membrane surface, while B and F are in a horizontal section. Bars indicate 0.2 mm. *(Continued)*

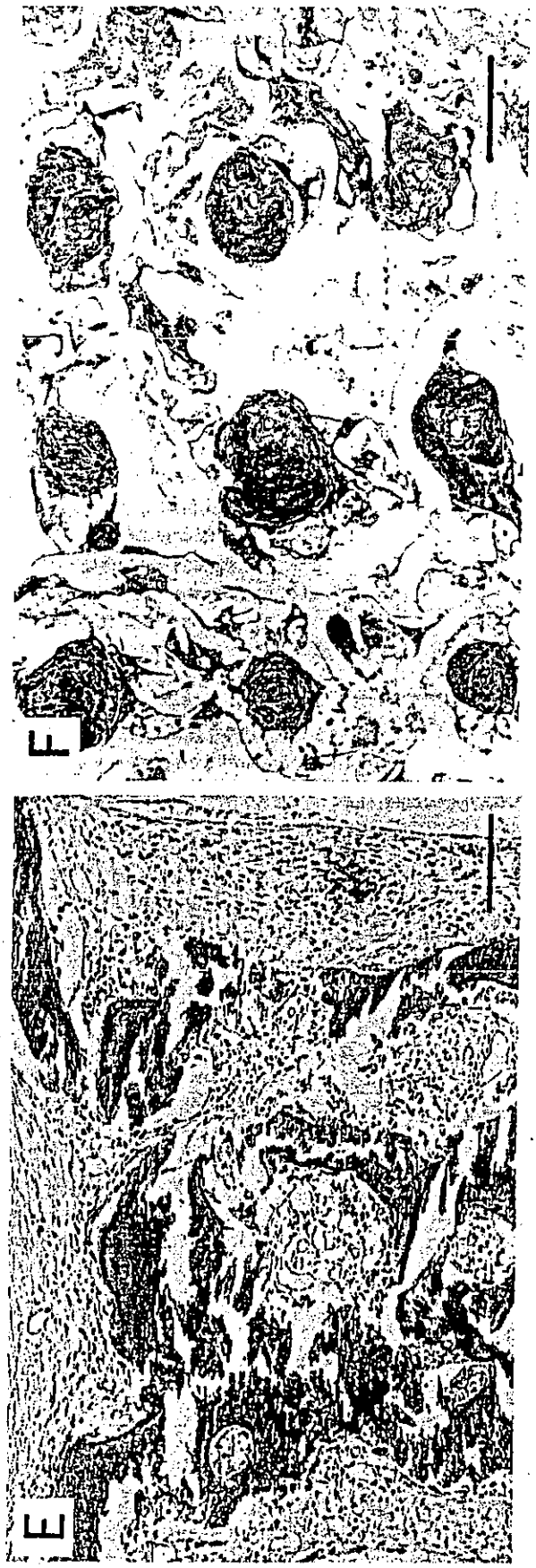

Figure 3. (Continued).

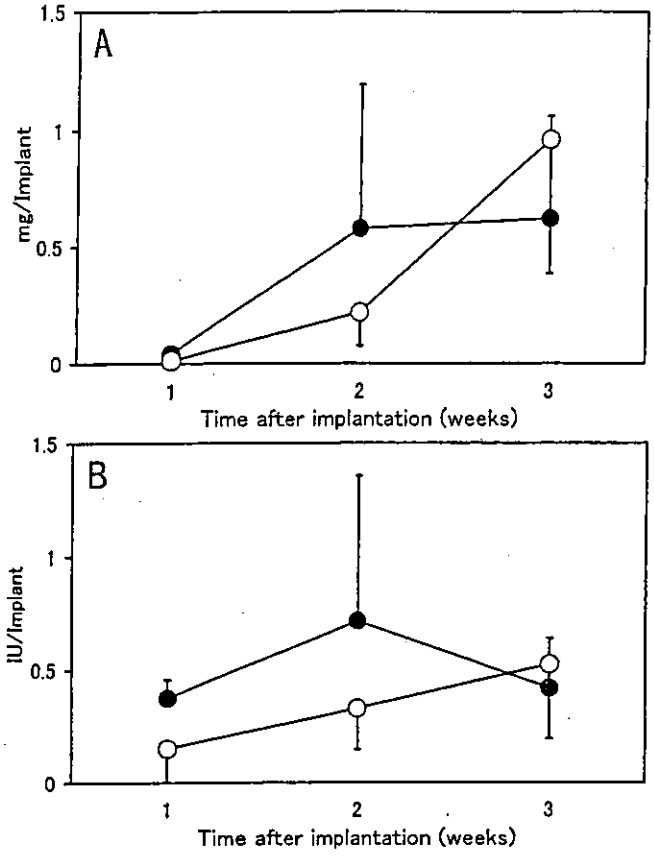

Figure 4. Time-dependent changes of calcium contents (A) and alkaline phosphatase activities (B) in the PLA-CL membranes with and without perforation. Solid circles indicate PLA-CL membrane with the pores 1.0 mm and open circles nonperforated membranes. There was a tendency of time-dependent increases in calcium contents and alkaline phosphatase activities in both perforated and nonperforated PLA-CL membranes. Statistical difference was significant between calcium contents of nonperforated PLA-CL at 1 and 3 weeks ($p < .05$). But there was no significant difference between the perforated groups and the nonperforated one.

in the middle of the pore (Figure 3A). It was clear that the orientations of fibers (or fiber bundles) in the 0.2 mm and 1.0 mm pores were different, when we randomly examined 200 fibers and estimated their angles to the plane parallel to the membrane in each pore. Preliminary results indicated more than 85% of the discernable fibers or bundles were at 90 ± 10° in 0.2 mm pores, and less than 35% were in 1.0 mm pores.

DISCUSSION

We were the first to apply the laser perforation technique to a BMP carrier [4]. One of the advantages of laser perforation technology is that we can precisely control the size and geometric distribution of pores. Porosity of membranous BMP carriers is important because it affects both the retention of the cytokine and the anchorage of the recruited mesenchymal cells [3–7]. With this expectation, we could demonstrate that the laser-perforated collagen films, particularly ones with pore sizes larger than 0.5 mm, induced higher amounts of bone than the nonperforated membranes [4].

Concerning the laser-perforated PLA-CL membrane with the pores of 1 mm, we histologically observed cartilage formation at 1 week (Figure 3B) and bone formation at 2 weeks and thereafter (Figure 3A, 3E). In addition, a significant time-dependent increase in the calcium content was observed in the nonperforated PLA-CL membranes (Figure 4). However, clear differences in calcium contents or alkaline phosphatase activities were not confirmed between the perforated and nonperforated PLA-CL membranes in this study. This was probably because this sponge-type PLA-CL membrane already had a porous structure before laser perforation, which was created by the salt leaking method (85% porosity). The porous structure could clearly be seen in the scanning electron microscopy profiles of this membrane (Figure 1A–1D). Actually in the histological sections, the small fissures and holes with 5–50 μm sizes, other than the laser-perforated pores, were occupied by cells, blood vessels, and bone tissues (Figure 3F).

The most remarkable morphological feature seen in the PLA-CL membranes was the active orientated fiber formation along the ring-type pores (0.2 mm in width) and the pores 0.2 mm in diameter. Bone formation seemed to occur on these collagenous matrices (Figure 3C). The active orientated fiber formation seemed to be guided by the continuous longitudinal pore structure of 0.2 mm in these PLA-CL membranes, and probably by the rough surface geometry of this material. The fiber-directing function of the PLA-CL membrane with the pores of 0.2 mm is expected to be useful in carriers of BMP and other cytokines for the tissue engineering of periodontal regeneration.

Another interesting difference between both carriers of collagen films and PLA-CL membrane was in their modes of osteogenesis. In previous observation of the perforated collagen films, bone formation always occurred on the surface of the film [4], whereas in the perforated PLA-CL membrane osteogenesis started mostly upon the newly formed collagenous matrix and seldom occurred on the surface (Figure 3A, 3C, 3F). Early mineralization seen in X-ray photographs (Figure 2) may not necessarily correspond to bone formation. Thus, Haversian system-like bone formation, which was clearly seen in the perforated collagen films [4] and in the porous hydroxyapatite BMP-carriers [1, 7, 14], was not observed in the PLA-CL membrane except in rare cases. The difference can be explained by the chemical and geometrical factors of the collagen films and the PLA-CL membrane.

Studies of the sustained release from PLA-CL of cisplatin, an anticancer agent, and other low molecular weight substances, verified significant affinity to this copolymer [12]. But the affinity of PLA-CL to BMP remains to be studied. On the other hand, the geometrical properties of both carriers were obviously different. There are numerous fissures or holes, inside and also on the surface of the PLA-CL membrane (Figure 1A–D and Figure 3), which might give a less congenial environment for cell attachment than the smooth surface of collagen film.

REFERENCES

[1] Kuboki, Y., Jin, Q.-M., and Takita, H. (2001). Geometry of carriers controlling phenotype expression in BMP-induced osteogenesis and chondrogenesis. *J. Bone Joint Surg.* 83-A:S1-105–115.

[2] Kuboki, Y., Takita, H., Mizuno, M., and Fujisawa, R. (2001). Geometry of artificial extracellular matrices: A new paradigm from dental tissue engineering. *Dent. Japan* 37:42–50.

[3] Mahmood, J., Takita, H., Ojima, Y., Kobayashi, M., Kohgo, T., and Kuboki, Y. (2001). Geometric effect of matrix upon cell differentiation: BMP-induced osteogenesis using a new bioglass with a feasible structure. *J. Biochem.* 129:163–171.

[4] Kikuchi, M., Takita, H., Nakayama, Y., Matsuda, T., and Kuboki, Y. (2000). Laser-perforated collagen membrane: Pore size-dependent bone induction of a new BMP carrier. *J. Hard Tiss. Biol.* 9:79–89.

[5] Jin, Q.M., Takita, H., Kohgo, T., Atsumi, K., Itoh, H., and Kuboki, Y. (2000). Effects of geometry of hydroxyapatite as a cell substratum. *J. Biomed. Mater. Res.* 51:491–499.

[6] Kuboki, Y., Takita, H., Kobayashi, D., Tsuruga, E., Inoue, M., Murata, M., Nagai, N., Dohi, Y., and Ohgushi, H. (1998). BMP-induced osteogenesis on the surface of hydroxyapatite with geometrically feasible and non feasible structures: Topology of osteogenesis. *J. Biomed. Mater. Res.* 39:190–199.

[7] Tsuruga, E., Takita, H., Itoh, H., Wakisaka, Y., and Kuboki, Y. (1997). Pore size of porous hydroxyapatite as the cell-substratum controls BMP-induced osteogenesis. *J. Biochem.* 121:317–324.

[8] Kuboki, Y., Saito, T., Murata, M., Takita, H., Mizuno, M., Inoue, M., Nagai, N., and Poole, A.R. (1995). Two distinctive BMP carriers induce zonal chondrogenesis and membranous ossification, respectively: Geometrical factors of matrices for cell differentiation. *Connect. Tiss. Res.* 32:219–226.

[9] Reddi, A.H. (1981). Cell biology and biochemistry of endochondral bone development. *Coll. Rel. Res.* 1:209–226.

[10] Kuboki, Y., Sasaki, M., Saito, A., Takita, H., and Kato, H. (1998). Regeneration of periodontal ligament and cementum by BMP-applied tissue engineering. *Eur. J. Oral Sci.* 106:197–203.

[11] Kuboki, Y., Watanabe, K., Kikuchi, M., Takita, H., Sato N., Fujinaga, T., Kato H., and Ohata. N. (1998). Periodontal regeneration in the reimplanted tooth by BMP-applied tissue engineering. 76th General Session and Exhibition of the IADR. *J. Dent. Res.* 77, abstract #1027.

[12] Wada, R., Hyon S.-H., Nakamura, T., and Ikada, Y. (1991). In vitro evaluation of sustained drug release from biodegradable elastomer. *Pharm. Res.* 8:1292–1296.

[13] Nakayama, Y., Anderson, J.M., and Matsuda T. (2000). Laboratory-scale mass production of a multi-micropatterned grafted surface with different polymer regions. *J. Biomed. Mater. Res.* 53:584–591.

[14] Kuboki, Y., Jin, Q. M., Kikuchi, M., Mamood, J., and Takita, H. (2002). Geometry of artificial ECM: Sizes of pores controlling phenotype, expression in BMP-induced osteogenesis and chondrogenesis. *Connect. Tiss. Res.* 43:529–534.

[15] Takita, H., and Kuboki, Y. (1997). Carrier-dependency and synergism in BMP-induced bone formation. *J. Hard. Tis. Biol.* 7:37–40.